Journal of Materials Chemistry A

Accepted Manuscript

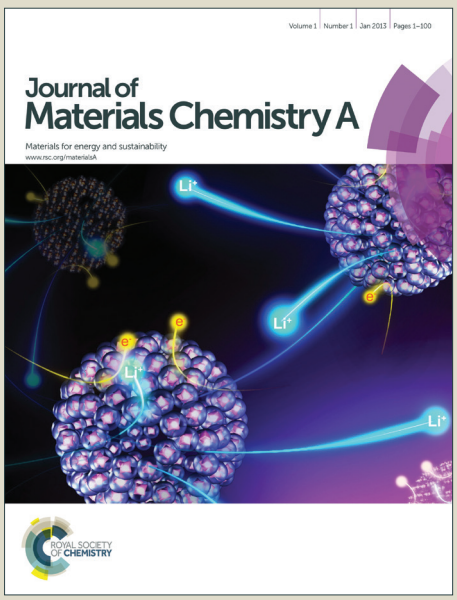

ROYAL SOCIETY OF CHEMISTRY

www.rsc.org/materialsA

Standing Carbon-Coated Molybdenum Dioxide Nanosheets on Graphene: Morphology Evolution and Lithium Ion Storage Properties

Lei Guo and Yong Wang*

Department of Chemical Engineering, School of Environmental and Chemical Engineering, Shanghai University, Shangda Road 99, Shanghai, P. R. China, 200444

Phone: +86-21-66137723. Fax: +86-21-66137725. Email: yongwang@shu.edu.cn

Abstract

Transitional metal oxides are a class of high-capacity anodes for lithium ion batteries. Drastic volume changes during cycling and intrinsic poor electronic conductivity diminish their electrochemical performances such as cycliability and high-rate performances. This work reports an unprecedented MoO_2/carbon network consisting of the standing carbon-coated MoO_2 nanosheets on graphene nanosheets to solve these problems. The obtained MoO_2 products can be tuned to be particle-like, rod-like, and sheet-like morphologies (standing MoO_2@C core-shell nanosheets or flat-lying MoO_2 nanosheets) on graphene by adjusting experimental parameters. Due to the unique three dimensional porous MoO_2@C-graphene hierarchical structure, the composite manifests excellent electrochemical properties including high capacity, long cycle life and stable high-rate performances. A large reversible capacity of above 500 mAh g^{-1} can be achieved after 200 cycles at a large current of 5 A g^{-1}.

Keywords: core-shell, MoO_2, nanosheets, graphene, lithium ion batteries

Introduction

Rechargeable lithium-ion batteries (LIBs), as the popular electrochemical energy storage system, have been applied in the fields of portable electronic devices, hybrid electrical vehicles, and electrical vehicles. Development of electrode materials with satisfactory properties in terms of high capacity, long cycle life and good rate capability, have been the hot topic for next-generation LIBs.[1-3] Graphite, used as the conventional anode material, has a limited theoretical specific capacity of 372 mAh g^{-1}. Transition metal oxides have attracted significant research concerns due to their higher gravimetric and volumetric capacity. For example, MoO_2 possesses a high theoretical capacity of 838 mAh g^{-1}, which has been proposed as a promising anode candidate for lithium-ion batteries.[4-7] However, drastic volume change of MoO_2 and other transitional metal oxides during cycling gives rise to electrode pulverization and subsequently fast capacity decay.

Nanostructured electrode have been demonstrated to deliver better electrochemical performances than their bulky counterparts due to the shortened electronic and ionic diffusion pathway, larger active surface area, and enhanced reaction kinetics.[8-19] Hybridizing metal oxides with carbon materials (such as carbon coating[20-28] and carbon support[29-42]) is also an effective strategy to buffer the critical problem of volume change. Graphene, owing to its unique properties such as ultrahigh surface area, excellent thermal and electronic conductivity, and highly flexible and robust structure, has been demonstrated as a good support for preparation of various graphene-based high-capacity composites.[33-40,43-48] MoO_2 nanostructures with diverse morphologies including nanoparticle[8-9], nanosheet[10], nanorod[11-13], nanotube[14-15], mesoporous structure[16-17], and core-shell structure[18-19] have been synthesized and explored as anodes for Li-ion

batteries. Moreover, MoO_2-carbon nanocomposites such as carbon-coated MoO_2[20-28], MoO_2/mesoporous carbon[29-30], MoO_2/carbon nanotube[31-32], and MoO_2/graphene[33-40] with enhanced electrochemical performances have been reported recently. It is worth noting that MoO_2 has been fabricated with nanoparticle morphology in most MoO_2/graphene reports[33-40], while MoO_2 nanorods can be obtained on graphene in a single report[37]. Graphene supported MoO_2 nanoparticles can be also self-assembled into a rod-like nanostructure[40].

Herein, we develop a facile one-step thermolysis method for fabricating two-dimensional graphene supported four types of MoO_2 morphologies and explore their morphology-dependent lithium-storage applications. The standing MoO_2@C nanosheet or flat-lying MoO_2 nanosheet on graphene, MoO_2/graphene rod-on-sheet and particle-on-sheet composites can be obtained by varying experimental conditions. Such a unique hierarchical graphene-based structure, namely the standing or flat-lying MoO_2 nanosheets on graphene has not been witnessed previously. The three dimensional porous structure of carbon-coated MoO_2 nanosheets erected on graphene is found to be a more suitable morphology as an anode for Li-ion batteries. It delivers a large capacity of 752 mAh g^{-1} after 100 cycles at a small current of 100 mA g^{-1} and remains a large capacity of 502 mAh g^{-1} after 200 cycles at an extremely large current of 5 A g^{-1}.

Experimental Section

Materials synthesis: All chemicals were used as received without further purification. Graphene nanosheets (GNS) were prepared by a modified Hummers method, followed by a thermal reduction as reported previously[44,48]. In a typical synthesis of MoO_2@C nanosheet/graphene sheet-on-sheet composite: GNS (0.036 g) and hexaammonium heptamolybdate (AHM, 0.05 g)

tetrahydrate were dissolved in ethanol (20 mL) and then sonicated for 30 min. The solid precursor was obtained by evaporating the ethanol solvent at 80 ^{o}C for 12 h and subsequently treated in a tube furnace at 550 ^{o}C for 2 h under flowing 40 sccm gas mixtures of 5% C_2H_2 and 95% N_2. To explore the effect of graphene in the composite, various amounts of GNS were also used for the preparation of MoO_2@C/Graphene sheet-on-sheet composites with different loadings of MoO_2.

MoO_2/Graphene sheet-on-sheet and particle-on-sheet composites were prepared in a similar preparation process by replacing 5% C_2H_2/N_2 with pure N_2 or 5% H_2/N_2 respectively. A mixture of MoO_2/Graphene rod-on-sheet and particle-on-sheet structures was prepared in 5% C_2H_2/N_2 by replacing AHM with phosphomolybdic acid (PMA) hydrate. MoO_2@C product was prepared by a similar method in the absence of GNS.

Materials characterization: The obtained products were characterized by X-ray diffraction (XRD, Rigaku D/max-2550V, Cu Kα radiation), field-emission scanning electron microscopy (FE-SEM, JSM-6700F) with an energy dispersive X-ray spectrometer (EDS), transmission electron microscopy and high-resolution transmission electron microscopy (TEM, HRTEM, JEOL JEM-200CX and JEOL 2010F). Raman spectroscopy was recorded on Renishaw in plus laser Raman spectrometer (excitation wavelength: 785 nm, excitation power: 3 mW, spot size: ~1.2 μm). The Brunauer-Emmett-Teller (BET) surface area and porous structures were measured by an accelerated surface area and porosimetry analyzer (Micromeritics Instrument Corp, ASAP 2020 M + C, analysis adsorptive: N_2). Thermogravimetric analysis (TGA) was performed on a NETZSCH STA 409 PG/PC instrument under air atmosphere at a ramp rate of 10 ^{o}C min^{-1}.

Electrochemical measurements: The Swagelok-type cells were assembled in an argon-filled glove-box and used to measure the electrochemical performances. The working electrodes were composed of active material, acetylene black and poly (vinylidene difluoride) (PVDF) at a weight ratio of 80: 10: 10 in N-methyl pyrrolidinone (NMP). The loading amount of the electrode on copper foil was kept at ~2 mg cm^{-2} and the thickness was ~20 micrometers. The specific capacity was calculated based on the total weight of the composite electrode materials. Lithium foil was used as the reference electrode. The electrolyte was 1 M $LiPF_6$ dissolved in a mixture of ethylene carbonate (EC) and diethyl carbonate (DEC) (1: 1 w/w). The cells were discharged (lithium insertion) and charged (lithium extraction) at a constant current (100 mA g^{-1}, 0.1 C, 1 C = 1000 mA g^{-1}) in the fixed voltage range 5 mV to 3.0 V. Higher hourly rates (1, 5, or 10 C) were also used, and the first cycle discharging was kept at 0.1 C. Cyclic voltammetry (CV) was performed on a CHI660D electrochemical workstation at a scan rate of 0.1 mV s^{-1}. Nyquist plots were collected on the same workstation for various electrodes from 100 kHz to 0.01 Hz.

Results and Discussion

Scheme 1 illustrates the growth process of four distinct morphologies of MoO_2/Graphene composites all by a one-step facile thermolysis technique. MoO_2 particles are obtained on graphene in 5% H_2/N_2, while MoO_2 nanosheets are observed on graphene in pure N_2 gas. If C_2H_2 is used, carbon-coated MoO_2 (MoO_2@C) nanosheets are formed and erected on GNS. After stacking, these standing MoO_2 nanosheets on graphene would form a three dimensional porous MoO_2/Graphene layer-by-layer nanostructure, in which there is void space among standing MoO_2 nanosheets to accommodate the volume expansion and facilitate the charge transfer. On the other hand, graphene nanosheets are separated efficiently with large distance by these

standing MoO_2 nanosheets. Amorphous carbon coating from C_2H_2 decomposition is used as a binder to link MoO_2 and graphene and make the composite structure stable. The above three composites are all prepared using hexaammonium heptamolybdate (AHM) tetrahydrate as the precursor source of MoO_2. When another precursor of phosphomolybdic acid (PMA) hydrate is used under flowing C_2H_2, carbon coated MoO_2 with a mixture morphology of nanorods and nanoparticles are obtained as the final product on graphene.

Figure 1 shows SEM images of graphene nanosheets (GNS), MoO_2@C particles and the standing MoO_2@C nanosheets on graphene. Graphene is wrinkled and very thin under electron imaging (Figure 1a). MoO_2@C is prepared by the decomposition of AHM under flowing acetylene gas in the absence of graphene. Particles with irregular shape are observed and their surface is rather smooth, indicating a carbon overlayer may be present (Figure 1b). The carbon layer can be confirmed by the corresponding EDS spectrum in Figure 1c and elemental mapping images (Figure S1, Supporting Information). A uniform distribution of pyrolytic carbon layer from the decomposition of acetylene is present in MoO_2@C composite. Figure 1d-e show SEM images of graphene supported MoO_2@C nanosheets. Interestingly, a large number of small nanosheets are wrapped by graphene nanosheets and most nanosheets are found to stand on the graphene surface. These observed MoO_2 nanosheets interweave with graphene nanosheets, forming a sandwiched three dimensional porous network after stacking. Because MoO_2 nanosheets are erect rather than flat-lying on GNS, more open and porous spaces are introduced into the network of the packed MoO_2/graphene composite electrode. This will facilitate the diffusion of lithium ions and electrons and electrolyte infusion. The EDS spectrum and elemental mapping images for the standing MoO_2@C nanosheets on graphene are shown in Figure 1f and

Figure S2 of Supporting Information. A few elements such as Mo, C, and O are observed and distributed uniformly in the composite.

To further study the morphology and microstructure of the obtained products, TEM and HRTEM measurements are carried out. MoO_2@C sheets (~100-200 nm in size) are well wrapped by GNS (Figure 2a-c), which can increase the electrical conductivity and mechanical stability of MoO_2 and on the other hand, the agglomeration of GNS can be prevented by the sandwiched MoO_2@C nanosheets. It is of interest to note that most sheet-like MoO_2@C structures stand on GNS with different angles toward graphene substrate, although several nanosheets are still flat on GNS surface. A number of black lines (for example, one indicated by a white rectangle) can be observed in Figure 2b and 2c, which are the cross-section of standing MoO_2@C nanosheets under electron imaging because they are perpendicular to the graphene plane. Therefore the thickness of MoO_2@C nanosheets can be indicated by the width of these observed lines to be ~20 nm. The stable standing nanosheets on GNS should be ascribed to the supporting effect of pyrolytic carbon around MoO_2, which is formed by acetylene decomposition. This carbon layer functions as cement to link graphene and the standing MoO_2 nanosheets and make the integrated 3D composite network stable. The crystalline structure of MoO_2 and ultra-thin carbon shell are further characterized by HRTEM. As shown in Figure 2d, the lattice fringes of ~0.34 nm are observed, corresponding to the (110) plane of monoclinic MoO_2. The disordered carbon structure of graphene and carbon shell around MoO_2 core can be also observed in this image, therefore lithium ions can still intercalate easily through the outer carbon shell or graphene wrapping. Figure 2e shows the cross-section image of a standing MoO_2@C nanosheet chosen from Figure 2c, which is perpendicular to the graphene plane. There is clearly a carbon shell (~6-8 nm)

around MoO_2 in Figure 2e. In comparison, a flat-lying MoO_2@C nanosheet chosen from Figure 2c is shown in Figure 2f. The thickness of carbon shell is estimated to be ~3 nm, which is substantially smaller than that of the standing product as shown in Figure 2e. This should be ascribed to the different growth directions between standing and flat-lying MoO_2@C nanosheets. The standing MoO_2 nanosheet has more contact/reaction area with the flowing acetylene gas in the preparation process compared to the flat-lying MoO_2 nanosheet and therefore more acetylene may decompose around the erect nanosheet and form a thicker carbon layer. These HRTEM images provide direct evidences to confirm that most MoO_2 nanosheets grow erectly with the assistance of carbon shell. If there is no carbon shell or carbon shell is very thin, these nanosheets would tend to be flat on graphene surface.

Flat-lying MoO_2 sheets are also obtained by a similar thermolysis of AHM in pure N_2 instead of a mixture of C_2H_2/N_2. Figure 3a-c shows the MoO_2 sheets without carbon shell. They have an average size of ~100-200 nm, which is similar to that of MoO_2@C sheets. These observed MoO_2 sheets lie flat on graphene and no nanosheet stands on graphene surface. It is believed that nanosheet is more stable by larger face-to-face contact with graphene substrate because the thickness of nanosheet is only ~20 nm, which is much smaller than the size of the sheet (~100-200 nm). This also confirms the supporting effect of pyrolytic carbon for standing MoO_2@C nanosheets prepared in a C_2H_2-assisted thermolysis process. Nanosheets are unable to stand on graphene without the carbon support as shown clearly in Figure 3c. Figure 3d-f show the product prepared in H_2 instead of C_2H_2. A large number of MoO_2 nanoparticles are observed on GNS. These anchored MoO_2 particles are distributed uniformly with diameters of ~10-40 nm. Moreover, if PMA is used as the starting material instead of AHM, the morphology of

MoO_2/graphene composite is largely different. A number of small MoO_2 nanorods with lengths of ~100-200 nm and diameters of ~10-20 nm are wrapped in GNS layers (Figure S3, Supporting Information). TEM image in Figure S3c shows clearly the presence of many small MoO_2 nanoparticles (~5-10 nm) in the composite. Figure S4 in Supporting Information shows the effect of the reaction time on the final product. The morphologies of MoO_2@C sheets are roughly unchanged, but MoO_2@C nanosheets are not formed completely compared to the main product as shown in Figure 2. These tattered nanosheets exhibit smaller size of ~100-150 nm after shorter reaction time. Based on the above discussion, the experimental conditions such as the gas atmosphere, the starting precursor, and reaction time all have important influences on the shape and size of the obtained MoO_2 crystals.

Figure 4a shows XRD patterns of various products, all diffraction peaks of (110), (020), (220), (031), (-231) can be easily indexed to monoclinic MoO_2, which are in good agreement with the standard data (PDF 65-5787) [35]. The sharp and intense peaks suggest the formation of highly crystalline MoO_2. For several MoO_2/C composites, the characteristic (002) peak for graphite is not obvious, which should be ascribed to the low graphitic extent and the peak may be diminished by the strong (110) peak of MoO_2 at a similar position. Notably, MoO_3 are usually obtained by the decomposition of hexaammonium heptamolybdate (AHM) tetrahydrate in air, however the presence of carbon or reducing gas can reduce MoO_3 to MoO_2.[36,37] Thermogravimetric analysis of MoO_2/Graphene composites is carried out under air atmosphere at a ramp rate of 10 $^oC\ min^{-1}$ (Figure 4b). There is a small weight increase observed around 350-400 ^oC. This is mainly due to the oxidation of MoO_2 to MoO_3, which gains a theoretical weight increase of ~12.5 wt% (based on the mass of MoO_2). The decomposition of graphene occurs

around 380-460 ^{o}C and the solid residue is MoO_3. The MoO_2 contents in the composites can be calculated to be 48.3%, 54.2% and 53.2% for the standing MoO_2@C nanosheets on graphene, the flat-lying MoO_2 nanosheets on graphene and MoO_2/Graphene particle-on-sheet composites, respectively. It is worth noting that the carbon content of the standing MoO_2@C nanosheets on graphene is larger than the other two composites, which is ascribed to the formation of pyrolytic carbon in the standing MoO_2@C nanosheets on graphene. This extra amount of pyrolytic carbon coating can be estimated to be around 5.4% in the composite based on the increased amount of carbon (pyrolytic carbon and graphene) in MoO_2@C/Graphene compared to the average graphene amount in MoO_2/Graphene sheet-on-sheet and particle-on-sheet composites. Raman spectrum in Figure 4c displays both D-band at ~1320 cm^{-1} and G-band at ~1590 cm^{-1} for graphene and MoO_2/graphene composites. The D/G intensity ratios of the standing MoO_2@C nanosheets on graphene, the flat-lying MoO_2 nanosheets on graphene and MoO_2/Graphene particle-on-sheet are calculated to be 1.35, 1.33 and 1.31, which are all larger than bare graphene (1.18). It is indicated that hybridizing MoO_2 with graphene increases the content of disordered domains of graphene, which is caused by partially embedding of MoO_2 into graphene layer. These generated defects may be beneficial to the electrolyte infusion and lithium ion storage. Nitrogen adsorption-desorption isotherms of three MoO_2-graphene composites are shown in Figure 4d-f. Calculations based on isotherms show surface areas of 73.2, 132.2, and 136.2 m^2/g for the standing MoO_2@C nanosheets on graphene, the flat-lying MoO_2 nanosheets on graphene and MoO_2/Graphene particle-on-sheet composites, respectively. These composites display similar sharp ~3.2-3.8 nm mesopore peaks according to the inset pore size distribution curves. The smallest BET surface area of the standing MoO_2@C nanosheets on graphene reveals that a layer of pyrolytic carbon may be also present on graphene surface and therefore some

micro/meso-pores are closed by the carbon coating/coverage. Notably, lithium ion can still diffuse into these closed pores through the formed disordered carbon layer (as shown in HRTEM image of Figure 2e-f), therefore lithium-storage capacity should not be reduced.

CV curves of three MoO_2/Graphene composites at a scan rate of 0.1 mV s^{-1} are presented in Figure 5a. For the standing MoO_2@C nanosheets on graphene, two pronounced redox couples are observed at 1.49/1.78 V and 1.12/1.48 V which are corresponded to a reversible phase transition (reversible change between the orthorhombic and the monoclinic phase) of the partially lithiated Li_xMoO_2[13-14,16,49]. There is a broad peak at ~0.63 V, corresponding to the reduction of electrolyte and formation a solid electrolyte interface (SEI) film on the surface of the anode. The flat-lying MoO_2 nanosheets on graphene and MoO_2/Graphene particle-on-sheet composites exhibit similar redox peaks in the CV curves with increased voltage positions. Two redox peak pairs at 1.46/1.74 V, 1.25/1.55 V and 1.45/1.72 V, 1.27/1.56 V can be identified for the flat-lying MoO_2 nanosheets on graphene and MoO_2/Graphene particle-on-sheet, respectively.

The first-cycle galvanostatic discharge (lithium insertion) and charge (lithium extraction) curves of graphene, MoO_2@C (93.6% MoO_2), MoO_2/Graphene particle-on-sheet composite (53.2% MoO_2), the flat-lying MoO_2 nanosheets on graphene (54.2% MoO_2), and the standing MoO_2@C nanosheets on graphene (48.3% MoO_2, 5.4% carbon coating, and 46.3% graphene) are shown in Figure 5b. The standing MoO_2@C nanosheets on graphene exhibits initial discharge and charge capacities of 1255 mAh g^{-1} and 758 mAh g^{-1}, with a Coulombic efficiency of 60.4 %. The irreversible capacity loss in the first cycle should arise from irreversible lithium consumption and the formation of a solid electrolyte interface (SEI film) on the electrode surface. Two couples of

plateaus are clearly observed which are in good agreement with the CV results. In comparison, the initial discharge and charge capacities are 626 and 1102 mAh g^{-1} for the flat-lying MoO_2 nanosheets on graphene and 602 and 1095 mAh g^{-1} for the MoO_2/Graphene particle-on-sheet composite. The first discharge and charge capacities of MoO_2@C are only 263 and 370 mAh g^{-1}.

Figure 5c shows the cycling performances of various products at a current density of 100 mA g^{-1}. The MoO_2@C product shows a small reversible capacity of 161 mAh g^{-1} after 100 cycles. GNS has a slightly larger reversible capacity of 276 mAh g^{-1} after 100 cycles. In the presence of graphene, cycling performances are substantially improved for graphene/MoO_2 composites. The drastic volume change of MoO_2 during cycling process can be buffered by graphene and the restacking of graphene into graphite platelet can be prevented. The anode of the standing MoO_2@C nanosheets on graphene composite shows a large reversible capacity of 752 mAh g^{-1} after 100 cycles with a capacity retention rate of 99.2% compared to the first-cycle value. An average capacity fading of 0.008% per cycle can be calculated, indicating the excellent cycliability for the composite. Compared to the standing MoO_2@C nanosheets on graphene composite, the other two composites show reduced reversible capacities. The flat-lying MoO_2 nanosheets on graphene composite has a capacity fading from 626 mAh g^{-1} to 472 mAh g^{-1} during 100 cycles. The MoO_2/Graphene particle-on-sheet composite has the worst cycling performance among three types of MoO_2/Graphene composites because a small reversible capacity of 433 mAh g^{-1} is retained after 100 cycles, corresponding to 71.9% of the initial value.

High-rate cycling performances of three types of MoO_2/graphene composites are compared in Figure 6 and Figure S5 of Supporting Information. Large current rates of 1, 5, 10 C (1 C = 1000

mAh g^{-1}) are used to measure their high-rate performances. In general, there is a fast capacity fading in the first five cycles for three composites. The observed capacities tend to increase slightly during 10-80 cycles and are quite stable during the following cycles (~80-200 cycles). The slightly-increased reversible capacities during long cycling are also observed in the aforementioned Figure 5c and previous reports[24,33,39-40]. This phenomenon has been ascribed to the gradual activation process of conversion reaction between MoO_2 and Mo and the improved Li-diffusion kinetics due to partial crystallinity degradation of the electrode to a more disordered electrode structure[33,40]. The standing MoO_2@C nanosheets on graphene composite exhibits high initial charge capacities of 730, 717, 560 mAh g^{-1} at 1, 5, and 10 C, respectively, which are superior than those of the flat-lying MoO_2 nanosheets on graphene (616, 590, 551 mAh g^{-1}), MoO_2/Graphene particle-on-sheet (613, 601, 547 mAh g^{-1}) and bare graphene (657, 362, 272 mAh g^{-1} as shown in Figure S6 of Supporting Information). Highly reversible Li-ion storage capacities can be observed after repetitive cycling for the MoO_2@C/Graphene sheet-on-sheet composite. For example, 587 and 502 mAh g^{-1} can be retained for the composite at 1 C and 5 C respectively after 200 cycles. In comparison, the flat-lying MoO_2 nanosheets on graphene exhibits smaller reversible capacities than the standing MoO_2@C nanosheets on graphene composite at high current rates, and their high-rate cycling performances are better than the MoO_2/Graphene particle-on-sheet composite. The smallest reversible capacities of 403, 298, and 222 mAh g^{-1} after 200 cycles are observed for the MoO_2/Graphene particle-on-sheet composite at current rates of 1, 5, and 10 C, respectively. To the best of our knowledge, the observed excellent high-rate performance (above 500 mAh g^{-1} during 200 cycles at 5 A g^{-1}) for the standing MoO_2@C nanosheets on graphene has not been witnessed previously in various MoO_2-based anodes[4-40].

The electrochemical impedance spectra of MoO_2/Graphene composites over the frequency were carried out to investigate the kinetics of the electrode (Figure S7). The semicircles in the medium frequency are believed to reflect the charge-transfer resistance (Rct). Based on the equivalent circuit, the charge-transfer resistance (Rct) of carbon-coated MoO_2 particle is determined to be 98.5 Ω, which decreases to 84.5 Ω for graphene supported MoO_2 nanoparticles. The value of Rct is further decreased to 77.3 Ω for the flat-lying MoO_2 nanosheets on graphene possibly due to the larger contact area between MoO_2 nanosheets and GNS compared to that of particle-on-sheet composite. The standing MoO_2@C nanosheets on graphene composite exhibits the smallest diameter in the semicircle and a small resistance of 23.0 Ω can be determined. The fastest charge-transfer should be due to the multiple synergetic effects in the composite including sheet-like MoO_2 structure, graphene support, carbon coating, and the integrated 3D porous structure associated with the standing MoO_2 nanosheets on graphene.

The effect of weight ratio of MoO_2 to graphene is explored for optimizing the electrochemical performance for the standing MoO_2 nanosheets on graphene. Figure 7a-b and Figure S8 of Supporting Information show SEM images of the standing MoO_2 nanosheets on graphene composites with various loading amounts of MoO_2. It is clear that a suitable weight ratio of MoO_2 to graphene is crucial to the composite morphology. MoO_2 nanosheets can be still observed (Figure 7a-b and Figure S8a-d) in the range of MoO_2 loading from 34.7% to 71.9% (as calculated by TGA analysis in Figure 7c) and higher loading would lead to a heavy agglomeration of MoO_2 materials without sheet-like morphology on graphene (Figure S8e-f). Figure 7d and Figure S9 of Supporting Information compare the electrochemical performances

of the MoO_2@C/Graphene composites with different loading amounts of MoO_2. The initial charge/discharge capacities are 646/1219 and 482/909 mAh g^{-1} for MoO_2@C/Graphene (34.7% MoO_2) and MoO_2@C/Graphene (71.9% MoO_2) composites, respectively (Figure S9). The corresponding charge capacities are retained at 388 and 535 mAh g^{-1} after 100 cycles for two composites (Figure 7d). Therefore, these results demonstrate that the main product of MoO_2@C/Graphene (48.3% MoO_2) exhibits the best performance (752 mAh g^{-1} after 100 cycles) compared with the other two composites with higher or lower loading of MoO_2. It is suggested that the optimal value for MoO_2 must be between 34.7% and 71.9% and may be close to the main product of this work (48.3%). It is because that weight ratios of MoO_2 to GNS are bound up with the morphology, size and uniform distribution of MoO_2 on GNS. In the presence of high loading amount of GNS, the restacking of graphene may still take place because there are not sufficient "spacer" materials (MoO_2 nanosheets). On the contrary, in the presence of a small amount of GNS, MoO_2 materials are too crowded on GNS surface, in which the volume variation cannot be buffered efficiently by GNS. Figure S8e-f of Supporting Information show the MoO_2@C/Graphene composites with high loading of MoO_2 (85.7% and 95.2% MoO_2). The obtained MoO_2 in Figure S8f is similar to that of MoO_2@C in the absence of GNS and no sheet-like morphology can be observed.

The excellent cycling performances of the standing MoO_2 nanosheets on graphene composite should be ascribed to the 3D porous hierarchical nanostructure. Carbon coating and graphene support both have beneficial effects for enhanced electrochemical properties, which have been explored extensively in previous efforts.[20-28,33-40] The increased electrical contact, the improved mechanical stability, and the facilitated lithium diffusion have been usually determined for

carbon coating[20-28] and graphene support[33-40]. Besides these effects, it is emphasized here that carbon coating can help MoO_2 achieve a novel standing orientation on GNS surface. The resultant 3D porous hierarchical network in the electrode can exhibit more open and porous space and therefore facilitate the charge transfer and electrolyte infusion. These void spaces among erect MoO_2 nanosheets are also useful to accommodate the large volume expansion during cycling. Moreover, the erect MoO_2 nanosheets have two-sides of the exposed faces for lithium insertion and extraction. The restacking of graphene is also prevented more efficiently by the erect MoO_2 nanosheets between two neighboring graphene nanosheets in this 3D porous hierarchical nanostructure. The cycled composite electrode was examined again by XRD patterns (Figure S10a) and TEM image (Figure S10b). The initial crystalline MoO_2 structure has changed to be amorphous after 100 cycles and the standing sheet structure can be still observed despite the presence of PVDF binder and carbon black.

Conclusion

In summary, this work reports several MoO_2-grahphene morphologies: graphene supported MoO_2 nanoparticles, MoO_2 nanorods, and two unprecedented MoO_2 nanostructures (MoO_2 nanosheets and standing MoO_2@C core-shell nanosheets on graphene) by adjusting experimental conditions of a facile one-pot thermolysis approach. The growth mechanism of various MoO_2-based nanostructure and their morphology-dependent Li-ion storage properties are also explored. Excellent cycling performances at both small and high current densities are achieved for the standing MoO_2 nanosheets on graphene composite. Large reversible capacities of above 500 mAh g^{-1} can be delivered during 200 discharge-charge cycles at an extremely large current of 5 A g^{-1}.

Acknowledgements

The authors gratefully acknowledge the follow-up Program for Professor of Special Appointment in Shanghai (Eastern Scholar), the National Natural Science Foundation of China (51271105), and Innovative Research Team (IRT13078) for financial support. The authors also thank Lab for Microstructure, Instrumental Analysis and Research Center, Shanghai University, for materials characterizations.

Supporting Information Available:

Elemental Mapping, SEM, TEM, XRD and Electrochemical performance of MoO_2 based composites.

References

[1] A. Manthiram, J. Phys. Chem. Lett. 2011, 2, 176.

[2] Z. Y. Zhou, N. Tian, J. T. Li, I. Broadwell and S. G. Sun, *Chem. Soc. Rev.* 2011, **40**, 4167.

[3] C. M. Sim, Y. J. Hong and Y. C. Kang, *ChemSusChem* 2013, **6**,1320.

[4] Y. L. Liu, H. Zhang, P. Ouyang, W. H. Chen, Y. Wang and Z. C. Li, *J. Mater. Chem. A* 2014, **2**, 4714.

[5] Y. M. Sun, X. L. Hu, J. C. Yu, Q. Li, W. Luo, L. X. Yuan, W. X. Zhang and Y. H. Huang, *Energy Environ. Sci.* 2011, **4**, 2870.

[6] J. H. Ku, J. H. Ryu, S. H. Kim, O. H. Han and S. M. Oh, *Adv. Funct. Mater.* 2012, **22**, 3658.

[7] J. Liu, S. S. Tang, Y. K. Lu, G. M. Cai, S. Q. Liang, W. J. Wang and X. L. Chen, *Energy Environ. Sci.* 2013, **6**, 2691.

[8] Y. L. Liu, H. Zhang, P. Ouyang and Z. C. Li, *Electrochim. Acta* 2013, **102**, 429.

[9] J. H. Ku, Y. S. Jung, K. T. Lee, C. H. Kim and S. M. Oh, *J. Electrochem. Soc.* 2009, **156**, A688.

[10] L. C. Yang, Q. S. Gao, Y. H. Zhang, Y. Tang and Y. P. Wu, *Electrochem. Commun.* 2008, **10**, 118.

[11] D. Koziej, M. D. Rossell, B. Ludi, A. Hintennach, P. Novák, J. D. Grunwaldt and M. Niederberger, *Small* 2011, **7**, 377.

[12] X. Zhang, X. Z. Zeng, M. Yang and Y. X. Qi, *Eur. J. Inorg. Chem.* 2014, **2014**, 352.

[13] B. K. Guo, X. P. Fang, B. Li, Y. F. Shi, C. Y. Ouyang, Y. S. Hu, Z. X. Wang, G. D. Stucky and L. Q. Chen, *Chem. Mater.* 2012, **24**, 457.

[14] H. J. Zhang, J. Shu, K. X. Wang, X. T. Chen, Y. M. Jiang, X. Wei and J. S. Chen, *J. Mater. Chem. A* 2014, **2**, 80.

[15] H. J. Zhang, K. X. Wang, X. Y. Wu, Y. M. Jiang, Y. B. Zhai, C. Wang, X. Wei and J. S. Chen, *Adv. Funct. Mater.* 2014, **24**, 3399.

[16] Y. F. Shi, B. K. Guo, S. A. Corr, Q. H. Shi, Y. S. Hu, K. R. Heier, L. Q. Chen, R. Seshadri and G. D. Stucky, *Nano Lett.* 2009, **9**, 4215.

[17] X. P. Fang, B. K. Guo, Y. F. Shi, B. Li, C. X. Hua, C. H. Yao, Y. C. Zhang, Y. S. Hu, Z. X. Wang, G. D. Stucky and L. Q. Chen, *Nanoscale* 2012, **4**, 1541.

[18] X. F. Zhang, X. X. Song, S. Gao, Y. M. Xu, X. L. Cheng, H. Zhao and L. H. Huo, *J. Mater. Chem. A* 2013, **1**, 6858.

[19] X. Y. Zhao, M. H. Cao, B. Liu, Y. Tian and C. W. Hu, *J. Mater. Chem.* 2012, **22**, 13334.

[20] B. Liu, X. Y. Zhao, Y. Tian, D. Zhao, C. W. Hu and M. H. Cao, *Phys. Chem. Chem. Phys.* 2013, **15**, 8831.

[21] Y. M. Sun, X. L. Hu, W. Luo and Y. H. Huang, *J. Mater. Chem.* 2012, **22**, 425.

[22] Z. Y. Wang, J. S. Chen, T. Zhu, S. Madhavi and X. W. Lou, *Chem. Commun.* 2010, **46**, 6906.

[23] L. Zhou, H. B. Wu, Z. Y. Wang and X. W. Lou, *ACS Appl. Mater. Interfaces* 2011, **3**, 4853.

[24] H. J. Zhang, T. H. Wu, K. X. Wang, X. Y. Wu, X. T. Chen, Y. M. Jiang, X. Wei and J. S. Chen, *J. Mater. Chem. A* 2013, **1**, 12038.

[25] S. Yoon and A. Manthiram, *J. Mater. Chem.* 2011, **21**, 4082.

[26] W. Luo, X. L. Hu, Y. M. Sun and Y. H. Huang, *Phys. Chem. Chem. Phys.* 2011, **13**, 16735.

[27] Q. S. Gao, L. C. Yang, X. C. Lu, J. J. Mao, Y. H. Zhang, Y. Q. Wu and Y. Tang, *J. Mater. Chem.* 2010, **20**, 2807.

[28] L. C. Yang, L. L. Liu, Y. S. Zhu, X. J. Wang and Y. P. Wu, *J. Mater. Chem.* 2012, **22**, 13148.

[29] A. L. Chen, C. X. Li, R. Tang, L. W. Yin and Y. X. Qi, *Phys. Chem. Chem. Phys.* 2013, **15**, 13601.

[30] L. X. Zeng, C. Zheng, C. L. Deng, X. K. Ding and M. D. Wei, *ACS Appl. Mater. Interfaces* 2013, **5**, 2182.

[31] A. Bhaskar, M. Deepa and T. N. Rao, *ACS Appl. Mater. Interfaces* 2013, **5**, 2555.

[32] J. P. Jegal, H. K. Kim, J. S. Kim and K. B. Kim, *J. Electroceram.* 2013, **31**, 218.

[33] A. Bhaskar, M. Deepa, T. N. Rao and U. V. Varadaraju, *J. Power Sources* 2012, **216**,169.

[34] K. H. Seng, G. D. Du, L. Li, Z. X. Chen, H. K. Liu and Z. P. Guo, *J. Mater. Chem.* 2012, **22**, 16072.

[35] P. X. Han, W. Ma, S. P. Pang, Q. S. Kong, J. H. Yao, C. F. Bi and G. L. Cui, *J. Mater. Chem. A* 2013, **1**, 5949.

[36] Y. J. Chen, X. P. Di, C. Ma, C. L. Zhu, P. Gao, J. Q. Li, C. W. Sun and Q. Y. Ouyang, *RSC Adv.* 2013, **3**, 17659.

[37] Y. Xu, R. Yi, B. Yuan, X. F. Wu, M. Dunwell, Q. L. Lin, L. Fei, S. G. Deng, P. Andersen, D. H. Wang and H. M. Luo, *J. Phys. Chem. Lett.* 2012, **3**, 309.

[38] F. F. Xia, X. L. Hu, Y. M. Sun, W. Luo and Y. H. Huang, *Nanoscale* 2012, **4**, 4707.

[39] Q. W. Tang, Z. Q. Shan, L. Wang and X. Qin, *Electrochim. Acta* 2012, **79**, 148.

[40] Y. M. Sun, X. L. Hu, W. Luo and Y. H. Huang, *ACS Nano* 2011, **5**, 7100.

[41] P. Chen, F. D. Wu and Y. Wang, *ChemSusChem* 2014, **7**, 1407.

[42] Y. Gu, F. D. Wu and Y. Wang, *Adv. Funct. Mater.* 2013, **23**, 893.

[43] Y. Gu and Y. Wang, *RSC Adv.* 2014, **4**, 8582.

[44] J. Kan and Y. Wang, *Sci. Rep.* 2013, **3**, 3502.

[45] P. Chen, Y. Su, H. Liu and Y. Wang, *ACS Appl. Mater. Interfaces* 2013, **5**, 12073.

[46] L. Q. Lu, L. J. Lu and Y. Wang, *J. Mater. Chem. A* 2013, **1**, 9173.

[47] Y. Gu, Y. Xu and Y. Wang, *ACS Appl. Mater. Interfaces* 2013, **5**, 801.

[48] P. Chen, L. Guo and Y. Wang, *J. Power Sources* 2013, **222**, 526.

[49] J. R. Dahn and W. R. McKinnon, *Solid State Ionics* 1987, **23**, 1.

Figure Captions

Scheme 1. Schematic illustration showing the synthesis process of graphene supported various MoO_2 morphologies. The structure of standing carbon-coated MoO_2 (MoO_2@C) nanosheets on graphene is the main product of this work, which forms a sandwiched 3D porous network after stacking.

Figure 1. SEM images of (a) graphene, (b) MoO_2@C, (c) the EDS spectrum of MoO_2@C, (d-e) the standing MoO_2@C nanosheets on graphene at low and high magnifications, (f) the EDS spectrum of the standing MoO_2@C nanosheets on graphene.

Figure 2. TEM images of (a-c) the standing MoO_2@C nanosheets on graphene at different magnifications, HRTEM image of the standing MoO_2@C nanosheets on graphene showing (d) the MoO_2, carbon shell, and graphene, (e) a standing MoO_2@C core-shell nanosheet, (f) a flat-lying MoO_2@C core-shell nanosheet.

Figure 3. The flat-lying MoO_2 nanosheets on graphene: (a-b) SEM images and (c) TEM image, the MoO_2/Graphene particle-on-sheet composite: (d-e) SEM images and (f) TEM image.

Figure 4. Various MoO_2-based composites: (a) XRD patterns, (b) TGA curves, (c) Raman spectra. Nitrogen adsorption-desorption isotherms: (d) the standing MoO_2@C nanosheets on graphene, (e) the flat-lying MoO_2 nanosheets on graphene, (f) the MoO_2/Graphene particle-on-sheet composite.

Figure 5. Electrochemical performances of various MoO_2/Graphene composites: (a) CV curves, (b) the first-cycle discharge (lithium insertion) and charge (lithium extraction) curves, (c) cycling performance at a current density of 100 mA g^{-1} (0.1 C).

Figure 6. High-rate cycling performances of (a) the standing MoO_2@C nanosheets on graphene, (b) the flat-lying MoO_2 nanosheets on graphene, (c) the MoO_2/Graphene particle-on-sheet composite.

Figure 7. The MoO_2@C nanosheets on graphene with different amounts of MoO_2: (a) SEM image of the composite with 34.7 % MoO_2, (b) SEM image of the composite with 71.9 % MoO_2, (c) TGA curves, (d) cycling performance at a current density of 100 mA g^{-1} (0.1 C).

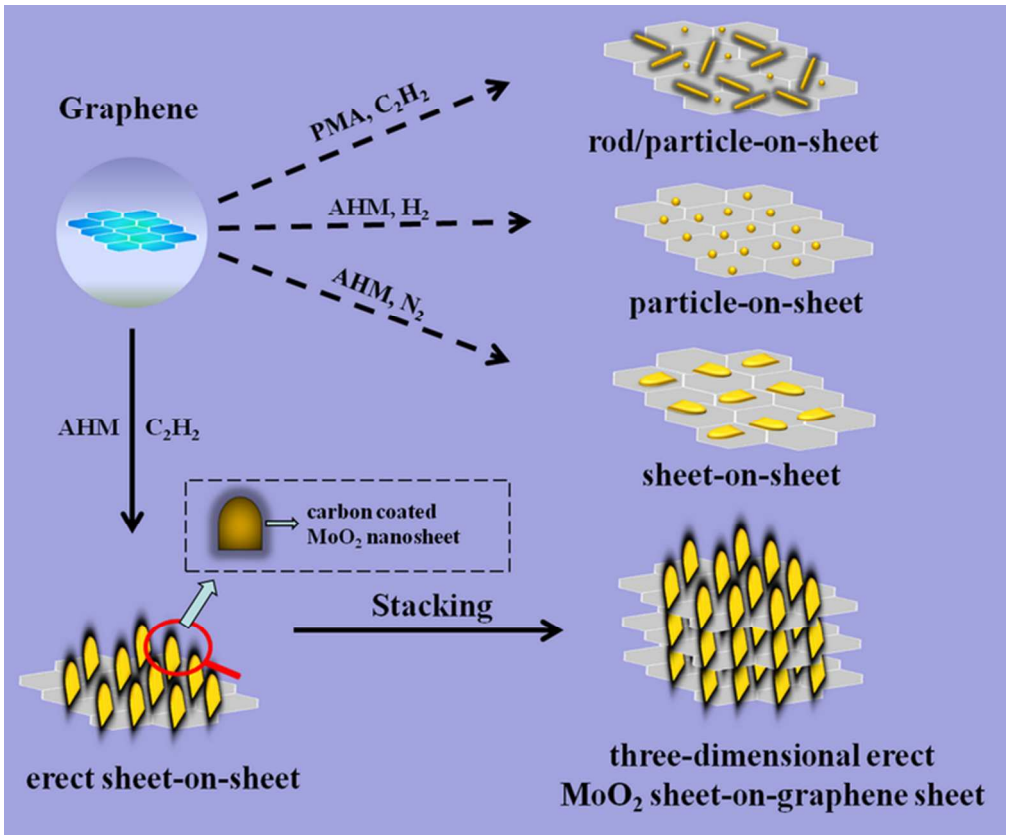

Scheme 1. Schematic illustration showing the synthesis process of graphene supported various MoO2 morphologies. The structure of standing carbon-coated MoO2 (MoO2@C) nanosheets on graphene is the main product of this work, which forms a sandwiched 3D porous network after stacking.
63x52mm (300 x 300 DPI)

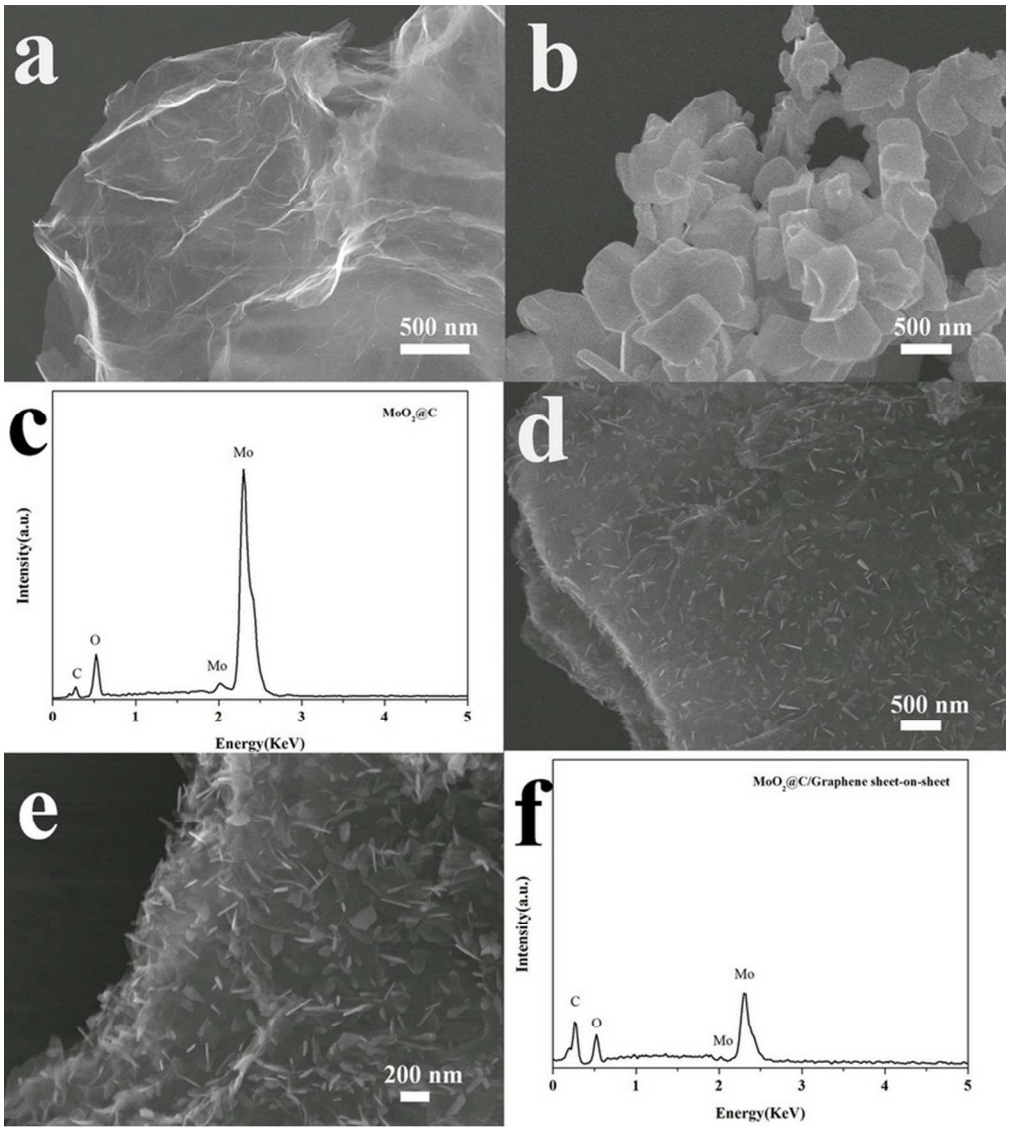

Figure 1. SEM images of (a) graphene, (b) MoO2@C, (c) the EDS spectrum of MoO2@C, (d-e) the standing MoO2@C nanosheets on graphene at low and high magnifications, (f) the EDS spectrum of the standing MoO2@C nanosheets on graphene.
70x78mm (300 x 300 DPI)

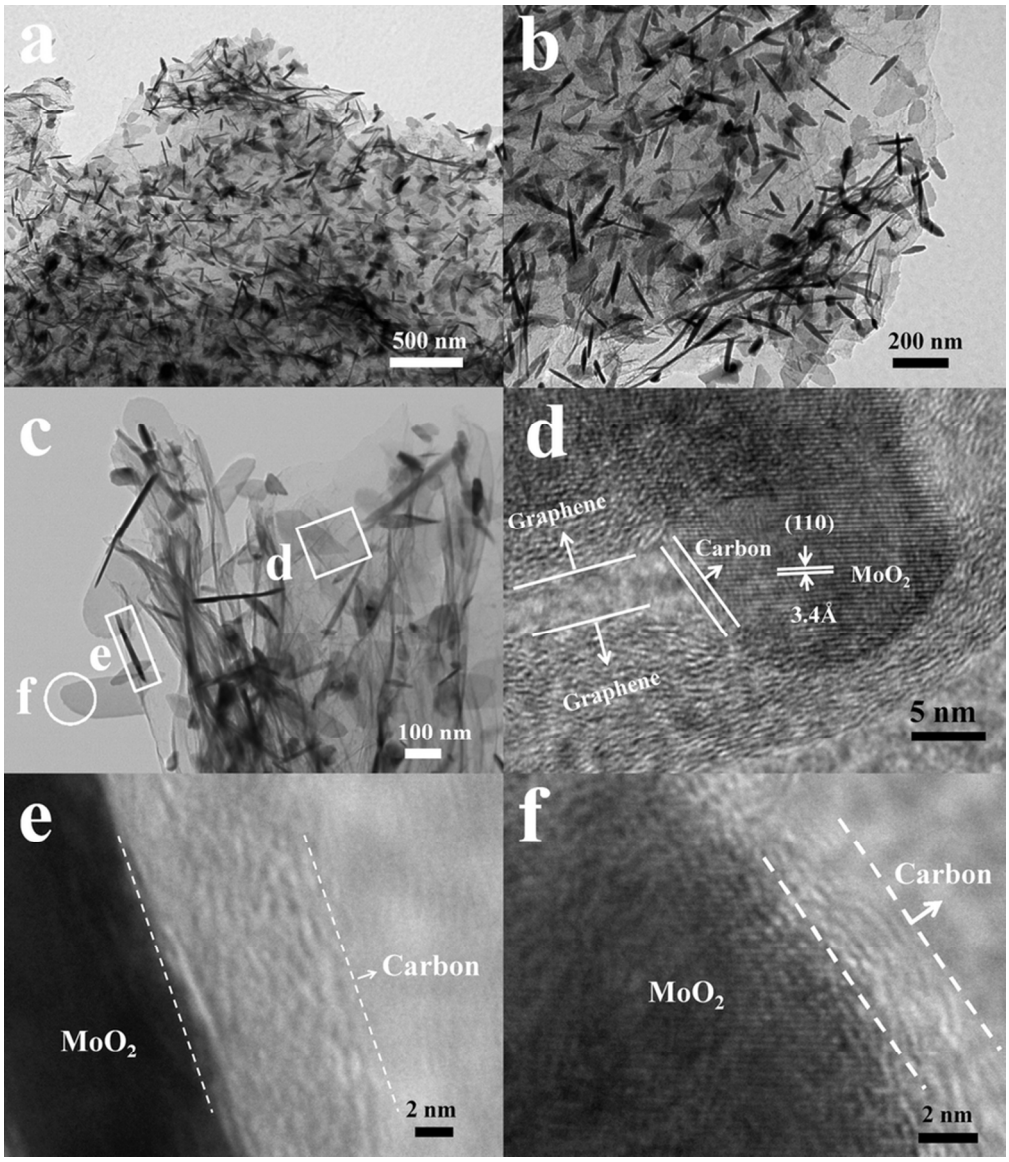

Figure 2. TEM images of (a-c) the standing MoO2@C nanosheets on graphene at different magnifications, HRTEM image of the standing MoO2@C nanosheets on graphene showing (d) the MoO2, carbon shell, and graphene, (e) a standing MoO2@C core-shell nanosheet, (f) a flat-lying MoO2@C core-shell nanosheet.
76x88mm (300 x 300 DPI)

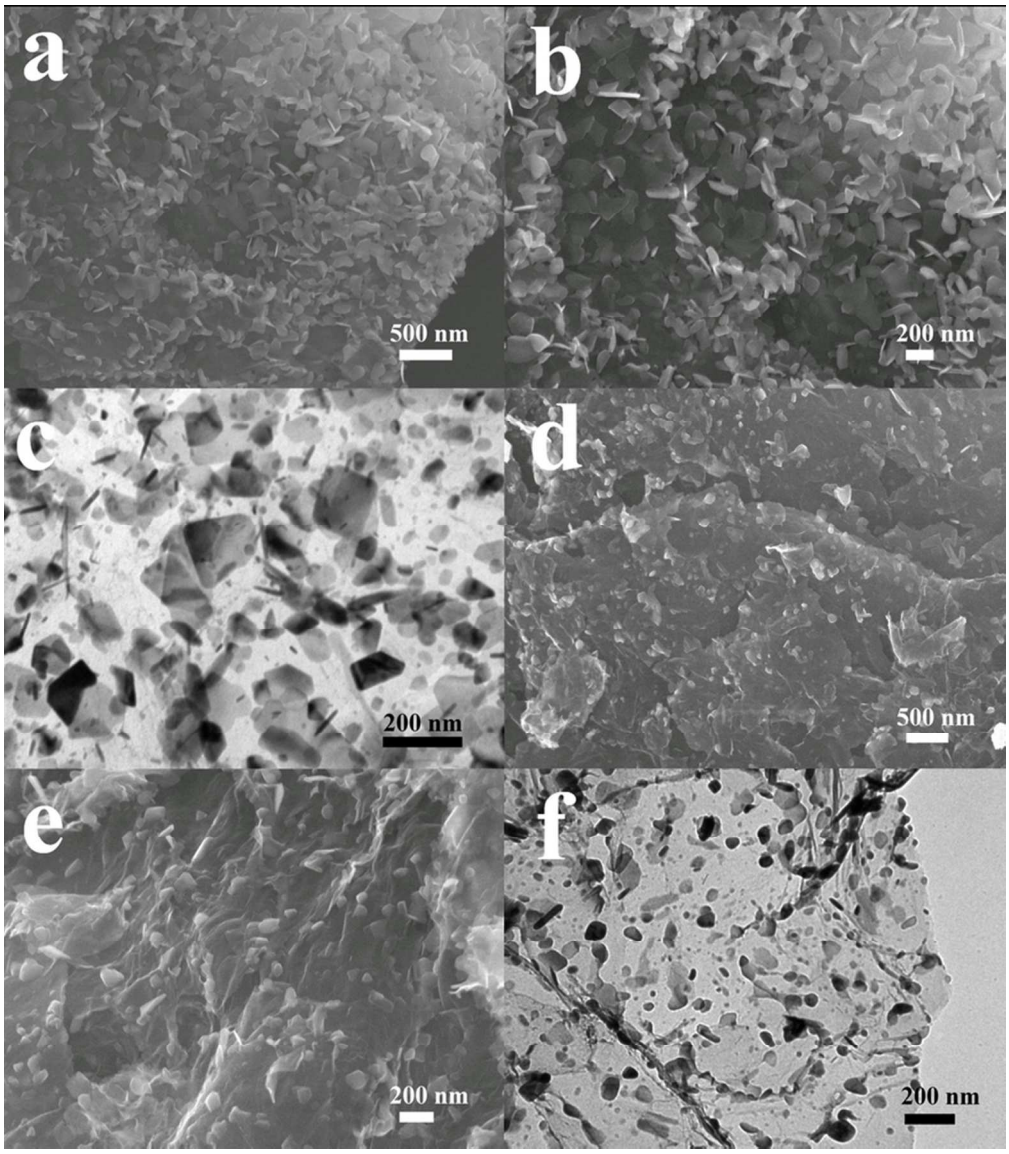

Figure 3. The flat-lying MoO2 nanosheets on graphene: (a-b) SEM images and (c) TEM image, the MoO2/Graphene particle-on-sheet composite: (d-e) SEM images and (f) TEM image.
74x84mm (300 x 300 DPI)

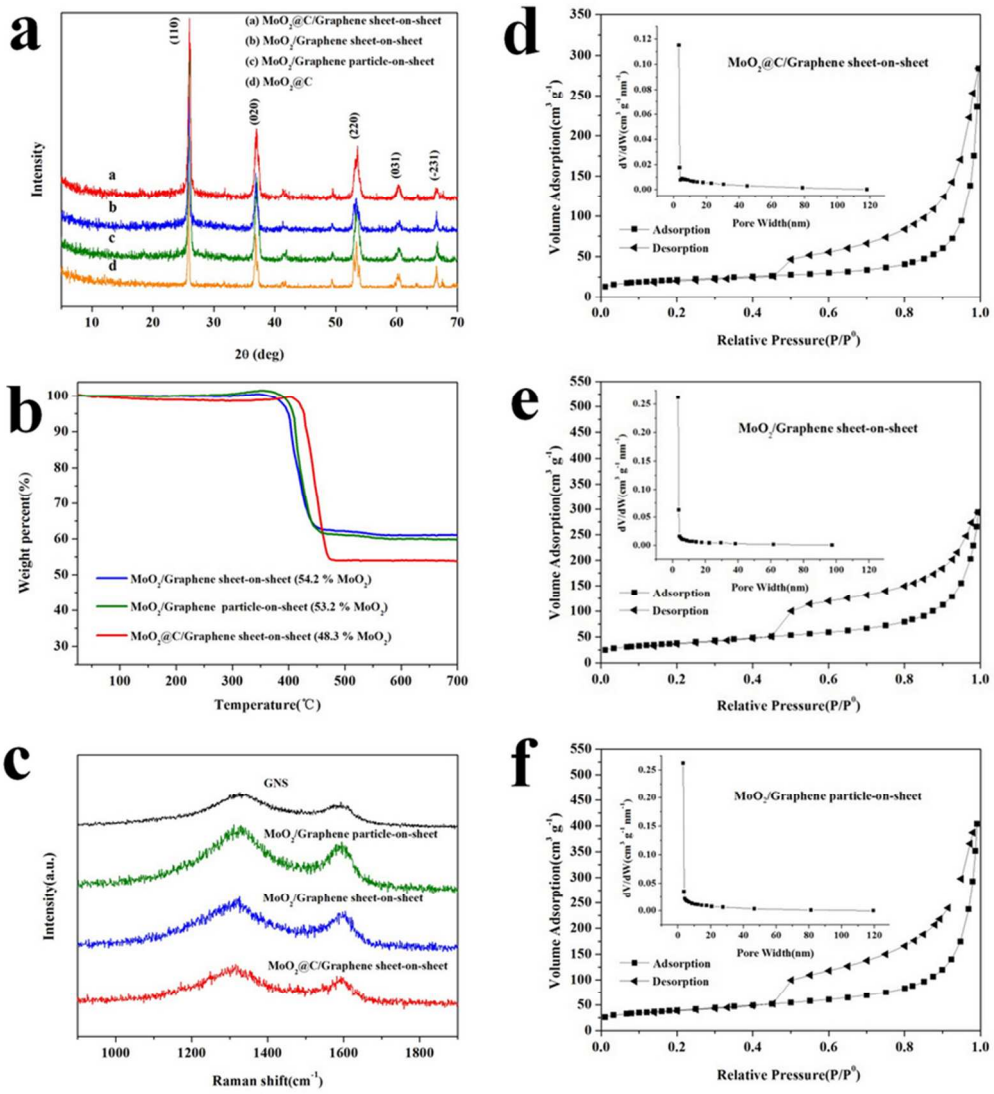

Figure 4. Various MoO2-based composites: (a) XRD patterns, (b) TGA curves, (c) Raman spectra. Nitrogen adsorption-desorption isotherms: (d) the standing MoO2@C nanosheets on graphene, (e) the flat-lying MoO2 nanosheets on graphene, (f) the MoO2/Graphene particle-on-sheet composite.
74x81mm (300 x 300 DPI)

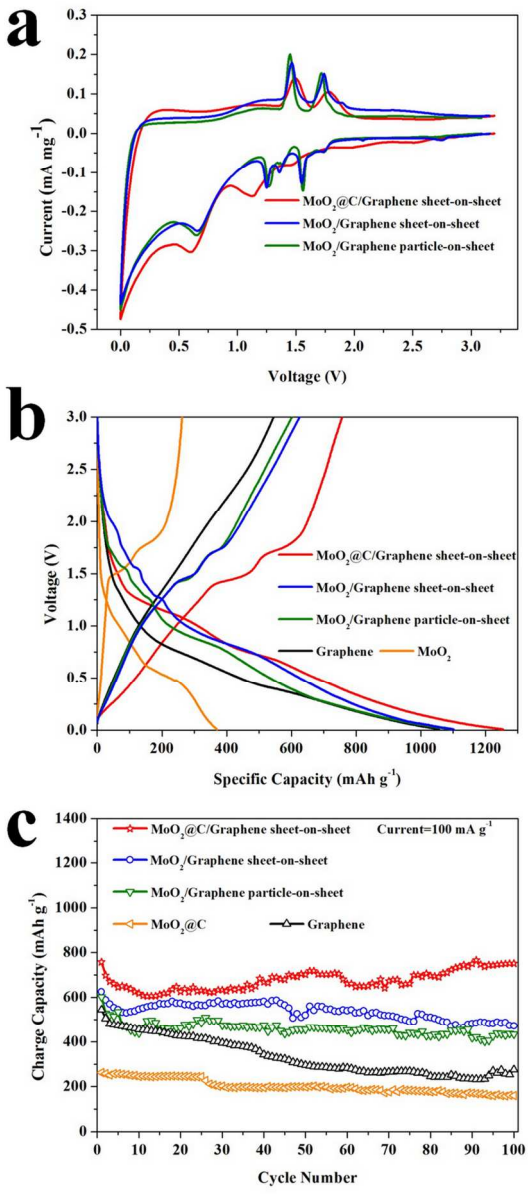

Figure 5. Electrochemical performances of various MoO2/Graphene composites: (a) CV curves, (b) the first-cycle discharge (lithium insertion) and charge (lithium extraction) curves, (c) cycling performance at a current density of 100 mA g-1 (0.1 C).
102x219mm (300 x 300 DPI)

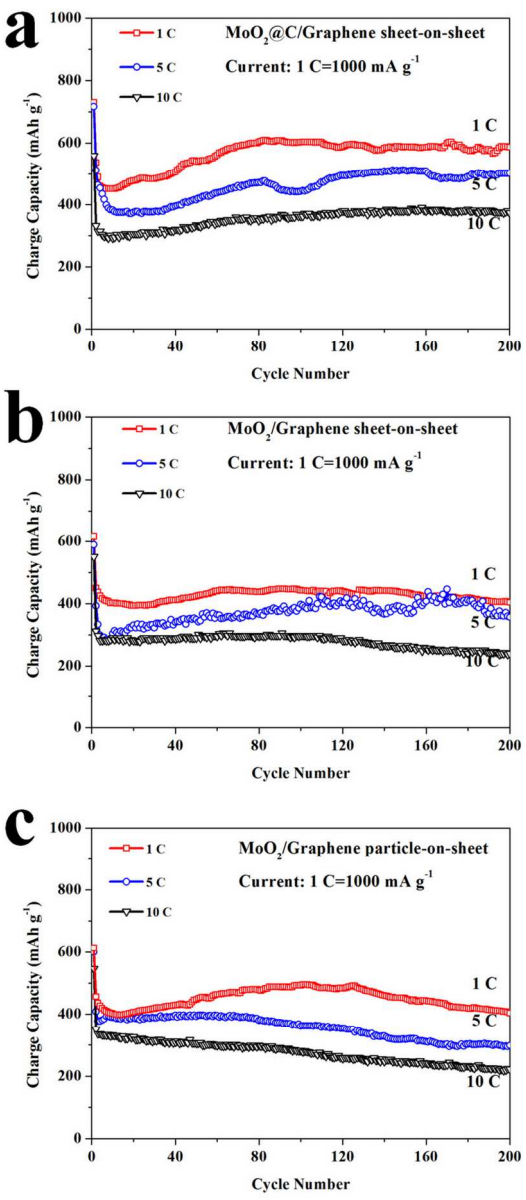

Figure 6. High-rate cycling performances of (a) the standing MoO2@C nanosheets on graphene, (b) the flat-lying MoO2 nanosheets on graphene, (c) the MoO2/Graphene particle-on-sheet composite.
103x222mm (300 x 300 DPI)

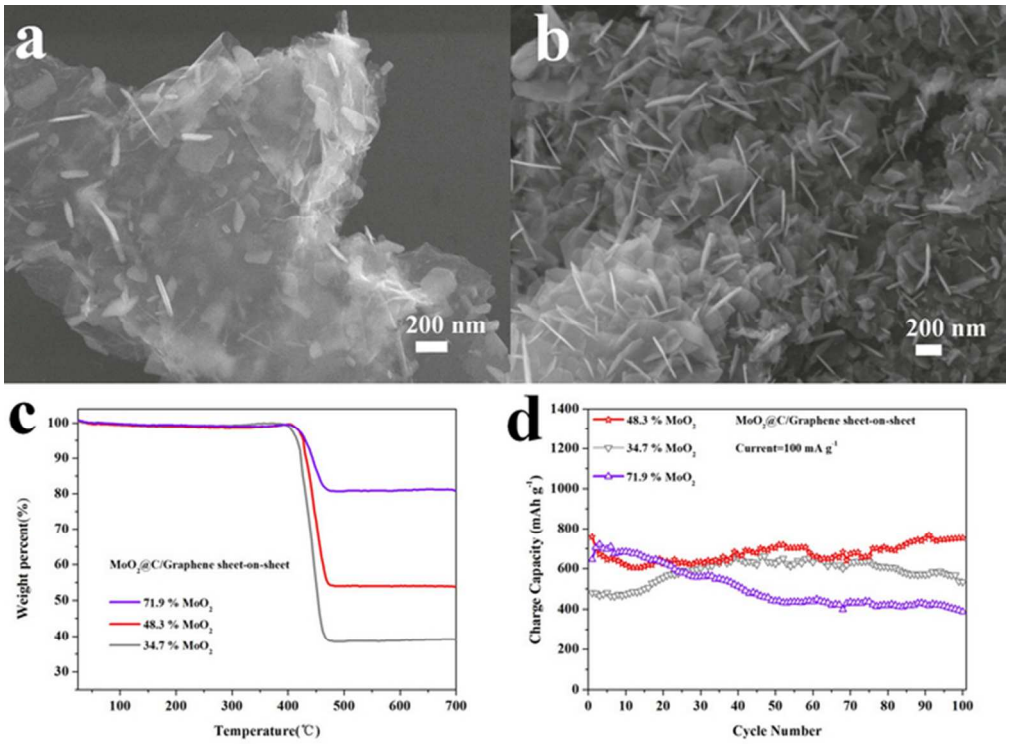

Figure 7. The MoO2@C nanosheets on graphene with different amounts of MoO2: (a) SEM image of the composite with 34.7 % MoO2, (b) SEM image of the composite with 71.9 % MoO2, (c) TGA curves, (d) cycling performance at a current density of 100 mA g-1 (0.1 C).
59x44mm (300 x 300 DPI)